

Optical Engineering

OpticalEngineering.SPIEDigitalLibrary.org

Regrowth-free single-mode semiconductor laser suitable for monolithic integration based on pits mirror

Mohamad Dernaika
Niall P. Kelly
Ludovic Caro
Kevin Shortiss
Frank H. Peters

SPIE.

Mohamad Dernaika, Niall P. Kelly, Ludovic Caro, Kevin Shortiss, Frank H. Peters, "Regrowth-free single-mode semiconductor laser suitable for monolithic integration based on pits mirror," *Opt. Eng.* **56**(8), 086107 (2017), doi: 10.1117/1.OE.56.8.086107.

Regrowth-free single-mode semiconductor laser suitable for monolithic integration based on pits mirror

Mohamad Dernaika,^{a,b,*} Niall P. Kelly,^{a,c} Ludovic Caro,^{a,c} Kevin Shortiss,^{a,c} and Frank H. Peters^{a,c}

^aTyndall National Institute, Integrated Photonics Group, Dyke Parade, Cork, Ireland

^bUniversity College Cork, Department of Electrical and Electronic Engineering, College Road, Cork, Ireland

^cUniversity College Cork, Department of Physics, College Road, Cork, Ireland

Abstract. A regrowth-free single-mode laser that is made using standard UV photolithography is reported. The laser achieves a single-mode side-mode suppression ratio of 37 dB, linewidth of 450 kHz, and tunes across 2.9 nm and is suitable for monolithic integration as a distributed feedback replacement, due to a large free spectral range of 60 nm. © The Authors. Published by SPIE under a Creative Commons Attribution 3.0 Unported License. Distribution or reproduction of this work in whole or in part requires full attribution of the original publication, including its DOI. [DOI: [10.1117/1.OE.56.8.086107](https://doi.org/10.1117/1.OE.56.8.086107)]

Keywords: photonic integrated circuit; single-mode laser; semiconductor lasers; lasers; photolithography; monolithic integration.

Paper 170694 received May 8, 2017; accepted for publication Aug. 2, 2017; published online Aug. 22, 2017.

1 Introduction

Distributed feedback (DFB) lasers have achieved commercial success in terms of supplying a stable single laser for wavelength-division multiplexing networks. However, they require multiple epitaxial regrowth steps, which increase the cost and add complexity to the fabrication process. Thus, surface-grating distributed Bragg reflector (DBR) lasers and laterally coupled DFB lasers fabricated using only a single epitaxial growth step have received considerable attention.^{1–8} However, they still require high-resolution lithography, such as electron beam (e-beam) or high-resolution holographic lithography, which adds to both process time and fabrication expense.

Regrowth-free semiconductor lasers that use standard contact UV lithography have been a subject of growing interest due to their potential to dramatically reduce the overall photonic components cost. These lasers achieve single-mode operation using various approaches, such as coupled cavities^{9,10} and multiple semiconductor ring lasers,^{11,12} or exploit mini reflections from index perturbation to create subcavities, such as slotted Fabry–Perot (SFP) lasers.^{13–15} They provide a high side-mode suppression ratio (SMSR) that can exceed 40 dB, a wide tuning range covering the C + L bands, fine tuning step <21 pm/mA,¹⁶ and output power over 25 mW.¹⁴ Moreover, in addition to their relatively simple fabrication process, they provide a narrow linewidth that has become a necessity for high spectral density, coherent optical communications.^{17,18} This low linewidth is generated without the need of an external cavity,¹⁹ complicated feedback system,²⁰ or dramatic increase in the cavity length as is typically required for DFB lasers to bring the linewidth down from a few MHz to the kHz regime. It is clear that there is a growing need for low-cost, compact, and narrow linewidth lasers that can be used in monolithic integration with other optical and optoelectronics components, such as modulators, amplifiers, and photodiodes.^{14,21–23}

In this paper, we demonstrate a regrowth-free higher order DBR laser process that does not require high-resolution photolithography. Mode selectivity is attained using a compact mirror with a length of 170 μm consisting of 1 $\mu\text{m} \times 1 \mu\text{m}$ deeply etched and closely spaced pits.²⁴ A small pit spacing was used to ensure a large (60 nm) free spectral range, which ensured that the laser operated in a narrow wavelength region (1 nm) over a large range of temperature and bias current. The laser achieves a single mode with an SMSR of 37 dB, a linewidth of 450 kHz and is thermally tunable across 2.9 nm. In addition, the laser is suitable for on-chip monolithic integration, as it can be implemented with or without a cleaved facet. Simulation results using the transmission matrix method (TMM)^{25–27} show a good agreement between theoretical and experimental data in predicting the behavior of the laser.

2 Laser Design and Fabrication

The laser consists of three sections for: gain, internal mirror, and absorption. The sections are electrically isolated using two shallow slots with a 7-deg angle to minimize reflections. An illustration of the laser design is shown in Fig. 1.

The gain section shown in Fig. 1 (red) is 600- μm long, and it is positioned between the mirror and a cleaved facet. The mirror section comprises 20, 25, or 30 deeply etched pits with a periodic spacing of 6 μm between the centers of the adjacent pits. The pits are deeply etched through the quantum wells, having one deep etch region extending over the pits. Similar to a shallow slot in an SFP laser, each pit produces a small reflection estimated at ~1% to 2% which then creates multiple subcavities. The multiple adjacent pits then generate enough optical feedback to form a mirror. All variants of the laser worked well; however, the 30-pit version generated the highest output power as well as the highest SMSR.

Pits were used instead of slots in this work because, unlike slots, the pits do not require an accurate etch depth to control the reflection power and bandwidth as described in Ref. 28. This eliminates the need for an etch stop with wet chemical etching to ensure consistency across the chip and over various fabrication runs. Moreover, avoiding the

*Address all correspondence to: Mohamad Dernaika, E-mail: mohamad.dernaika@tyndall.ie

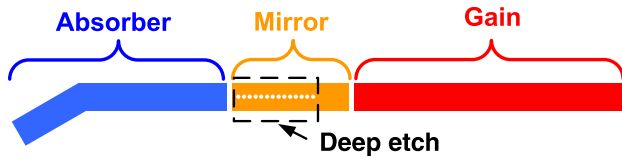


Fig. 1 Three-section laser design.

chemical etching eliminates the restriction on the cavity designs due to the influence of crystal orientation on the chemical etching.^{29,30} Furthermore, unlike the slot, the pit is compatible with high index contrast ridge waveguide structures.^{31,32} More details about the pit characteristics and features and comparison with a slot can be found in previous work.²⁴ Finally, the last part of the laser consists of a waveguide section with an angled cleaved facet (blue). As shown in Fig. 1, this part is labeled as absorber and it is mainly used as a light absorber while reverse biased. When unbiased, the angled facet can be used to collect light from the laser cavity. The angled facet significantly reduces the reflections from the semiconductor/air interface so it would not interfere with the main cavity. In this work, no high reflection or antireflection coatings were used.

Figure 2(a) shows a microscope image of the three-section laser and highlights the deep etch region surrounding the pits and the two isolation slots that divide the cavity into three electrically isolated sections. Figure 2(b) shows a scanning electron microscope image of a slice of the pit mirror.

The wafer material used in the process is commercial multiple quantum wells (MQW) material grown on an n-doped InP substrate. The MQW region consists of 5×6 nm strained QWs separated by 10×6 nm barriers. Two etch depths were used in the process. The shallow depth stops at 30 nm above the active region with the depth of $1.79 \mu\text{m}$, and it was used for the ridge and isolation slots. The deep etch goes through the active region to the n-doped layers reaching a depth of $2.9 \mu\text{m}$ and was used for the pits. A smooth side wall for both depths was realized using a $\text{CL}_2/\text{CH}_4/\text{H}_2$ inductively coupled plasma dry etch. The $2.5\text{-}\mu\text{m}$ -wide ridge side walls were passivated using 400-nm silicon dioxide. The 20:400 nm Ti:Au metal layer was e-beam evaporated for the p-metal contact. The substrate

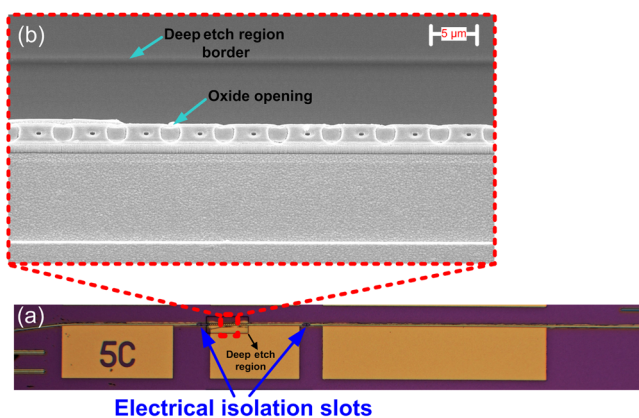


Fig. 2 (a) Microscope image and (b) SEM image of the pit mirror. Note that the larger circles between the pits are openings in the oxide to allow metal contacts with the ridge.

was then thinned to $100 \mu\text{m}$ using a bromine methanol solution. Finally, 20:250 nm Ti:Au was deposited for the n-contact on the back of the sample, which was then annealed at 380°C .

3 Results and Discussion

The laser was mounted on a temperature controlled brass chuck, and the light was collected from the straight cleaved facet via a lensed fiber. To characterize the laser performance, the light-intensity (L-I) curve of the laser was taken at various temperatures as shown in Fig. 3.

The L-I curves in Fig. 3 show a typical threshold trend of semiconductor lasers, which cause the laser threshold current to rise exponentially with temperature. The threshold-temperature dependency is mainly due to the rise of intrinsic losses in the active region at higher temperatures, which decrease the laser internal efficiency. The plots were taken by injecting 20 mA in the mirror section and sweeping the gain from 0 to 100 mA. Moreover, in order to make sure that the mirror is solely providing optical feedback without the help of the second facet, the absorber section of the laser was reverse biased to -3 V to absorb all the residual light. The laser lased in a single mode with an SMSR of 37 dB and a linewidth of 450 kHz is shown in Fig. 4.

Figure 4(a) shows the spectrum of the laser with peak wavelength at around 1535 nm with an SMSR of 37 dB. The inset in Fig. 4(a) is a close-up image of the single mode. Figure 4(b) shows the 900-kHz full width at half maximum of the measured electrical spectrum, which corresponds to a 450-kHz linewidth of the laser. The linewidth measurement was taken using a 50-km delayed self-heterodyne technique with a recirculating loop configuration and a resolution of <2 kHz.³³ Moreover, to further confirm the operation of the pit mirror, a fast Fourier transform (FFT) cavity analysis on the optical spectrum was performed. Figure 5(a) shows the cavity analysis based on the optical spectrum at lasing threshold [shown in Fig. 5(b)].

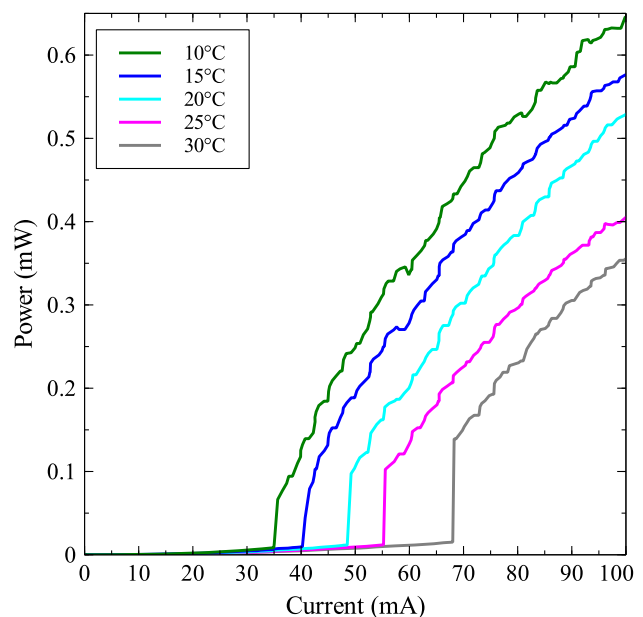


Fig. 3 L-I plot for different temperatures. The noise in data is caused by vibrations of the lensed fiber during data collection.

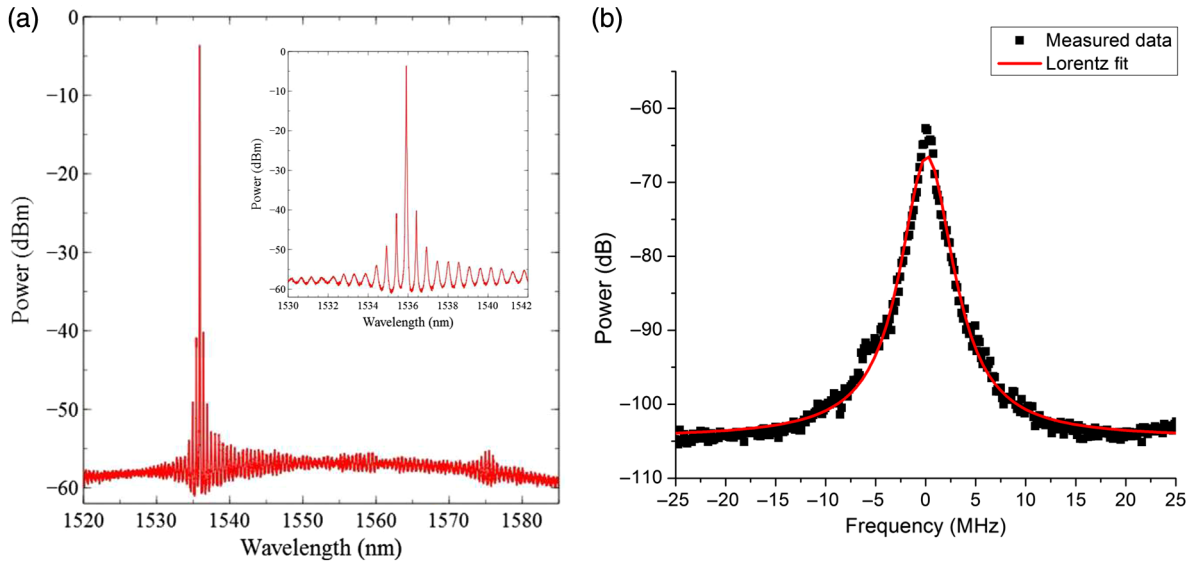


Fig. 4 (a) Spectrum with 37-dB SMSR and (b) linewidth measurement with Lorentz fit.

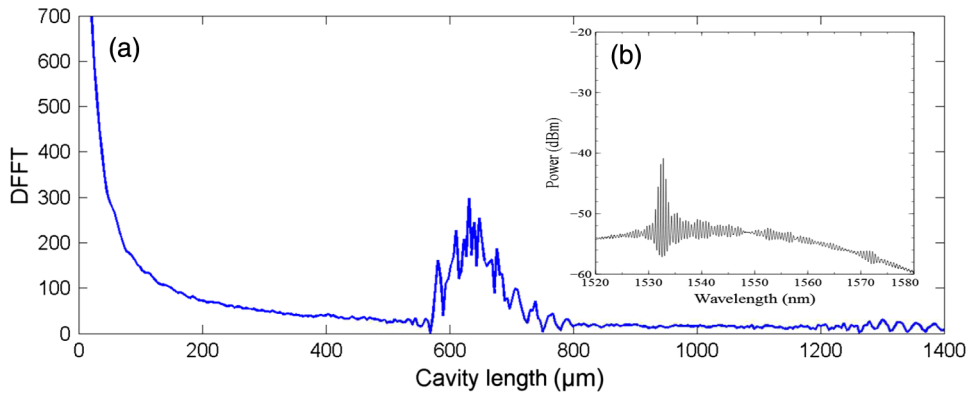


Fig. 5 (a) The cavity FFT spectrum and (b) laser spectrum at threshold.

The multiple peaks shown in Fig. 5(a) FFT represent the length of the subcavities created between the facet and each of the pits. No additional peaks can be seen at the full cavity length between the two facets at 1100 μm, proving that the absorbing section has fully isolated the cleaved angled facet from the lasing cavity. This confirms that the pit mirror can replace a cleaved facet and be used as a single-mode mirror for integration purposes as it is confirmed in Figs. 5(a) and 6.

Figure 6 shows the overlap spectrum of the coherent outputs of the laser from the two facets. The red spectrum is taken from the straight facet A, and the blue spectrum is taken from the angled facet B. The power taken from the left facet B is lower due to the low coupling efficiency between the angled facet and the lensed fiber and also due to the optical loss in this unbiased absorber section. However, the main purpose of facet B is to demonstrate that the laser can be integrated with other photonics components. Although, the demonstrated high-order DBR in this work uses a single cleaved facet, this cleaved facet can be easily replaced by broadband reflector, such as multimode interference reflector,³⁴ or a metal-coated-etched facet.³⁵ By doing so, the laser could be freely positioned anywhere on the chip to be used as facetless laser. Moreover, using a reflector with higher reflectivity than a uncoated cleaved

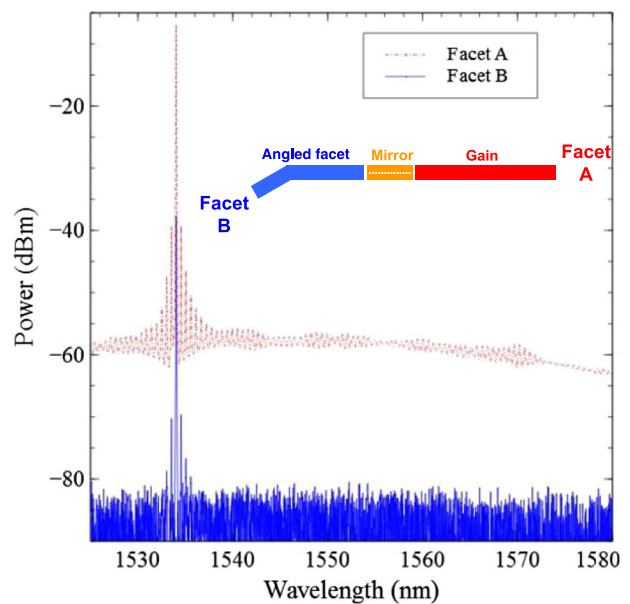


Fig. 6 The spectrum of the laser from the straight facet (red) and angled facet (blue).

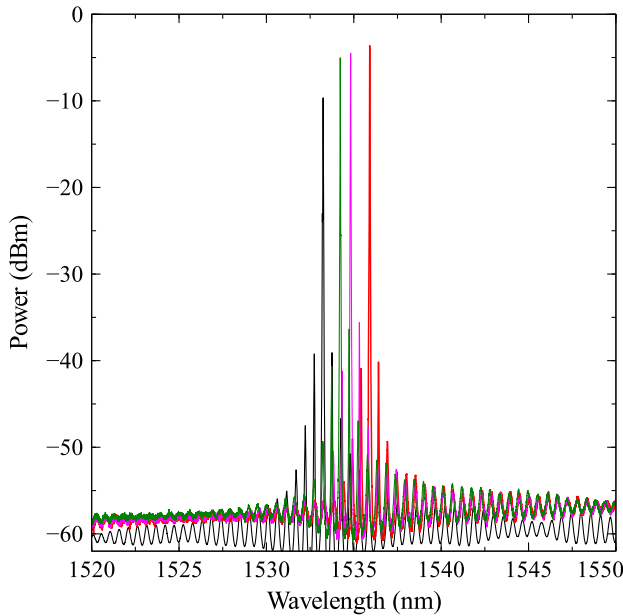


Fig. 7 Tuning across 2.9 nm.

facet ($\approx 30\%$) can potentially further improve the power efficiency and the linewidth of the laser. The single-mode output can be tuned across 2.9 nm by increasing injected current. The SMSR value is maintained above 30 dB over the tuning range. An overlap of the tuning spectrum is shown in Fig. 7.

4 Transmission Matrix Method Simulations

The wavelength selective reflection of the mirror section was modeled using a TMM technique, as described previously.²⁵ Each pit was taken to be a scattering point and assumed to reflect 3% of intensity while inducing a 15% loss. The reflection from facet A was taken to be 30%. Facet B was presumed not to contribute to the reflection, as the reverse biased section prior to facet B absorbed all the light traveling to and from the facet. This claim is supported by the lack of

a facet-to-facet resonance in Fig. 5(a). The transmission matrices for each scattering section i were of the form

$$T_{\text{Scat}} = \frac{1}{t_i} \begin{pmatrix} 1 & -r_i \\ -r_i & 1 \end{pmatrix}. \quad (1)$$

The field inside the device propagates as $e^{j\beta L}$, where L defines the propagation length and β is the propagation constant. The distance between the scattering points caused by the pits was taken to be $6.0 \mu\text{m}$ (the distance from the center of one pit to the next), with group index of the material assumed to be 3.45. The transmission matrices for the propagation sections were of the form

$$T_{\text{Prop}} = \begin{pmatrix} e^{j\beta L_i} & 0 \\ 0 & e^{-j\beta L_i} \end{pmatrix}. \quad (2)$$

Taking products of T_{Scat} and T_{Prop} , the resonant wavelengths of the device were calculated numerically. In Fig. 8(a), the resonance of the device is plotted on top of the measured spectrum. The positions of the lasing modes of the device were found to be accurately described by the transmission matrix model. At 1593 nm, the small rise of noise far from the gain peak is matched by the increase in reflection from the pit mirror section predicted by the model. Figure 8(b) demonstrates how the lasing wavelength can be controlled by changing the spacing between the pits. The graph shows various pit spacing between 3 and $6 \mu\text{m}$ and the resulting resonant wavelengths.

5 Conclusion

A regrowth-free higher order DBR laser has been demonstrated. The laser does not require high-resolution photolithography and achieves single-mode operation via a compact $170\text{-}\mu\text{m}$ mirror based on 30 deeply etched pits. The experimental results confirm that the laser is suitable for integration, and it can be fabricated using a single cleaved facet or as a facetless laser by replacing the cleaved facet with an integrated reflector. The single-mode output had

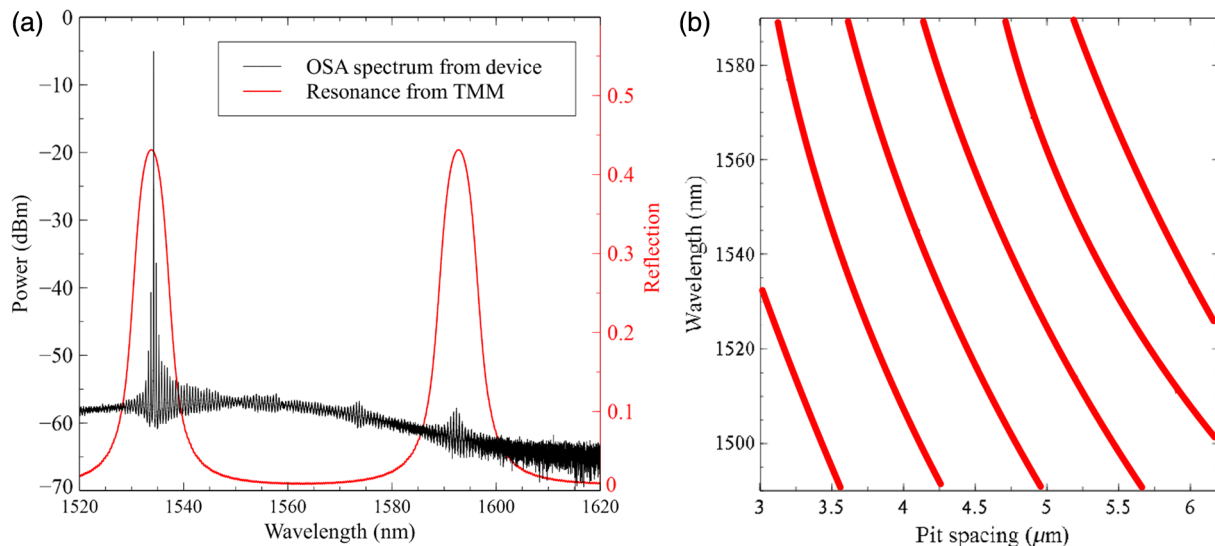


Fig. 8 (a) Simulated resonance of the laser cavity compared with the experimental spectrum of the laser and (b) lasing wavelength with various pit pit spacing.

an SMSR of 37 dB and a linewidth of 450 kHz with a tuning range of 3 nm. Finally, TMM simulation results agreed well with the experimental data in predicting the lasing behavior.

Acknowledgments

This work was supported by the Science Foundation Ireland under Grant Nos. SFI 13/IA/1960 and 12/RC/2276 (I-PIC). The author certifies that there is no actual or potential conflict of interest in relation to this article.

References

1. L. Miller et al., "A distributed feedback ridge waveguide quantum well heterostructure laser," *IEEE Photonics Technol. Lett.* **3**(1), 6–8 (1991).
2. N. Chen et al., "InGaAsP/InP laterally coupled distributed feedback ridge laser," *Jpn. J. Appl. Phys.* **39**(3S), 1508–1511 (2000).
3. S. Jang, J. Yu, and Y. Lee, "Laterally coupled DFB lasers with self-aligned metal surface grating by holographic lithography," *IEEE Photonics Technol. Lett.* **20**(7), 514–516 (2008).
4. Y.-H. Liu et al., "High efficiency, single-lobe surface-emitting DFB/DBR quantum cascade lasers," *Opt. Express* **24**(17), 19545–19551 (2016).
5. K. Papatryfonos et al., "Laterally coupled distributed feedback lasers emitting at 2 μm with quantum dash active region and high-duty-cycle etched semiconductor gratings," *J. Appl. Phys.* **121**(5), 053101 (2017).
6. S. Forouhar et al., "High-power laterally coupled distributed-feedback GaSb-based diode lasers at 2 μm wavelength," *Appl. Phys. Lett.* **100**(3), 031107 (2012).
7. L. Hou et al., "Laterally coupled dual-grating distributed feedback lasers for generating mode-beat terahertz signals," *Opt. Lett.* **40**(2), 182–185 (2015).
8. H. Duprez et al., "Hybrid III–V on silicon laterally coupled distributed feedback laser operating in the o-band," *IEEE Photonics Technol. Lett.* **28**(18), 1920–1923 (2016).
9. S. Zhang et al., "Simple and compact v-cavity semiconductor laser with 50 \times 100 GHz wavelength tuning," *Opt. Express* **21**(11), 13564–13571 (2013).
10. P. E. Morrissey et al., "Coupled cavity single-mode laser based on regrowth-free integrated MMI reflectors," *IEEE Photonics Technol. Lett.* **28**(12), 1313–1316 (2016).
11. S.-H. Kim et al., "Widely tunable coupled-ring reflector laser diode consisting of square ring resonators," *J. Opt. Soc. Korea* **14**(1), 38–41 (2010).
12. L. Wu et al., "Half-wave-coupled ring-FP laser with 50-channel 100-GHz-spaced wavelength tuning," *IEEE Photonics J.* **6**(4), 1–8 (2014).
13. Y. Zhang et al., "A hybrid silicon single mode laser with a slotted feedback structure," *Opt. Express* **21**(1), 877–883 (2013).
14. D. C. Byrne et al., "Discretely tunable semiconductor lasers suitable for photonic integration," *IEEE J. Sel. Top. Quantum Electron.* **15**(3), 482–487 (2009).
15. K. Shi et al., "Characterization of a tunable three-section slotted Fabry–Perot laser for advanced modulation format optical transmission," *Opt. Commun.* **284**(6), 1616–1621 (2011).
16. M. Dernaika et al., "Single facet semiconductor laser with deep etched v-notch reflectors integrated with an active multimode interference reflector," *J. Mod. Opt.* **64**, 1941–1946 (2017).
17. X. Xu et al., "Advanced modulation formats for 400-Gbps short-reach optical inter-connection," *Opt. Express* **23**(1), 492–500 (2015).
18. J. Pfeifle et al., "Flexible terabit/s Nyquist-WDM super-channels using a gain-switched comb source," *Opt. Express* **23**(2), 724–738 (2015).
19. T. Komljenovic et al., "Widely tunable narrow-linewidth monolithically integrated external-cavity semiconductor lasers," *IEEE J. Sel. Top. Quantum Electron.* **21**(6), 214–222 (2015).
20. W. Lewoczko-Adamczyk et al., "Ultra-narrow linewidth DFB-laser with optical feedback from a monolithic confocal Fabry–Perot cavity," *Opt. Express* **23**(8), 9705–9709 (2015).
21. H. Yang et al., "Monolithic integration of single facet slotted laser, SOA, and MMI coupler," *IEEE Photonics Technol. Lett.* **25**(3), 257–260 (2013).
22. J. Engelstaedter, B. Roycroft, and B. Corbett, "Laser and detector using integrated reflector for photonic integration," *Electron. Lett.* **44**(17), 1017–1019 (2008).
23. N. Kelly et al., "Regrowth-free integration of injection locked slotted laser with an electroabsorption modulator," *Opt. Express* **25**(4), 4054–4060 (2017).
24. M. Dernaika et al., "Deeply etched inner-cavity pit reflector," *IEEE Photonics J.* **9**(1), 1–8 (2017).
25. L. A. Coldren, S. W. Corzine, and M. L. Mashanovitch, *Diode Lasers and Photonic Integrated Circuits*, Vol. **218**, John Wiley & Sons, Hoboken, New Jersey (2012).
26. S. A. Dyakov et al., "Numerical methods for calculation of optical properties of layered structures," *Proc. SPIE* **7521**, 75210G (2010).
27. Q. Lu et al., "Analysis of slot characteristics in slotted single-mode semiconductor lasers using the 2-D scattering matrix method," *IEEE Photonics Technol. Lett.* **18**(24), 2605–2607 (2006).
28. W.-H. Guo et al., "Nine-channel wavelength tunable single mode laser array based on slots," *Opt. Express* **21**(8), 10215–10221 (2013).
29. N. Siwak, X. Fan, and R. Ghodssi, "Fabrication challenges for indium phosphide microsystems," *J. Micromech. Microeng.* **25**(4), 043001 (2015).
30. J. J. Kelly and H. G. Philipsen, "Anisotropy in the wet-etching of semi-conductors," *Curr. Opin. Solid State Mater. Sci.* **9**(1), 84–90 (2005).
31. D. Liang et al., "High-index-contrast oxide-confined GaAsP/InGaAsN multi-quantum-well ridge waveguide lasers," in *Conf. Digest, IEEE 20th Int. Semiconductor Laser Conf.*, pp. 165–166, IEEE (2006).
32. C. Seibert and D. Hall, "High-index-contrast ridge waveguide laser with thermally oxidised etched facet and metal reflector," *Electron. Lett.* **46**(15), 1077–1078 (2010).
33. H. Tsuchida, "Simple technique for improving the resolution of the delayed self-heterodyne method," *Opt. Lett.* **15**(11), 640–642 (1990).
34. E. Kleijn, M. K. Smit, and X. J. Leijtens, "Multimode interference reflectors: a new class of components for photonic integrated circuits," *J. Lightwave Technol.* **31**(18), 3055–3063 (2013).
35. N. P. Kelly et al., "Regrowth-free single mode laser based on dual port multimode interference reflector," *IEEE Photonics Technol. Lett.* **29**(3), 279–282 (2017).

Mohamad Dernaika is a PhD student at the University College Cork and with the Integrated Photonic Group, Tyndall National Institute. He received his master's degree in broadband telecommunication networks from the University of Hertfordshire in 2011. Between 2013 and 2015, he worked as a researcher in ultrafast fiber lasers with Photonic Research Center, Malaya University. His research interests include semiconductor lasers, photonic integrated circuits, injection locked lasers, and monolithic integration.

Niall P. Kelly is currently undertaking a PhD at Tyndall National Institute Cork. He received his BSc degree in applied physics from the University of Limerick in 2011, followed by the completion of his MSc degree from the University College Cork in 2013. His research interests include high-speed III–V optoelectronics components and photonic integrated circuits.

Ludovic Caro received a graduate generalist engineering degree from Ecole Catholique des Arts et Metiers Rennes and a research master's degree in electronics and telecommunications from Universite de Rennes 1, France, in 2014. Since 2015, he has been working on his PhD on lasers for photonic integrated circuits at Tyndall National Institute, Cork, Ireland.

Kevin Shortiss received a joint honors degree in mathematics and physics from University College Cork in 2015. Since then, he has been working on his PhD in physics at University College Cork, on injection locked semiconductor lasers as optical comb filters.

Frank H. Peters received his PhD from McMaster University, Canada, in 1991. He worked at the University of California, Santa Barbara, from 1991 to 1993, and then joined Optical Concepts from 1993 to 1996, followed by W. L. Gore and Associates from 1996 to 2000, Agilent Technologies from 2000 to 2001, and Infinera from 2001 to 2005, before moving to Ireland in 2005. He is now a professor in the Physics Department, University College Cork, and the head of the Integrated Photonics Group, the Tyndall National Institute.